2019 2nd IEEE International Conference on Soft Robotics (RoboSoft)
COEX, Seoul, Korea, April 14-18, 2019

High Force Generation Using Inflatable Toroidal Soft Robot Actuators

Josh Bishop-Moser[1]

Abstract— **Pneumatic and fluidic soft robotic actuators are often used for their force and motion generation capabilities, while leveraging the advantages of their soft construction, such as inherent compliance, low weight, and environmental adaptability. This paper presents a novel toroidal soft actuator design that produces increased force without increasing the external size of the actuator, the fluid pressure, or the strength of the materials holding the fluid. A model of the actuator is presented, relating design and operational parameters to axial force generation. A toroidal actuator is fabricated and compared to a McKibben actuator in axial force production. The experiments demonstrate that the toroidal design increases the force produced; in the prototype actuators, this force increase is approximately 45%. The forces estimated by the model are compared to the experimental results, and they are found to be representative, with only small errors.**

I. Introduction

Pneumatic and fluidic soft robotic actuators are often used for their force and motion generation capabilities, while leveraging the advantages of their soft construction, such as inherent compliance, low weight, and environmental adaptability. When used for force generation, the limiting factors are the size of the actuator (the diameter for cylindrical actuators), the fluid pressure, and the strength of the materials holding the fluid. Consequently, novel design topologies are needed to create higher force actuators without altering the diameter, pressure, or materials used. Fiber-reinforced actuators have demonstrated the ability to generate axial contraction forces that are many times higher than the product of their cross-sectional area and pressure. This is due to the mechanical advantage provided by a helical fiber-reinforcement structure. These actuators are generally known as Fiber-reinforced Elastomeric Enclosures (FREEs) and as McKibben actuators in the case where fiber reinforcement is of an equal and opposite angle. FREEs and McKibben actuators have been explored and modeled extensively for their force producing capacity [1] [2] [3] [4]. Approaches that have been investigated to generate more force in fluidic soft actuators include placing actuators in close proximity to each other in a parallel configuration [5] and using a vacuum actuation of bellow structures [6] [7]. Outside of fluid pressure, actuation methods such as nanotube yarn [8] have been investigated for improved force production.

This paper models and experimentally validates a toroidal topology to generate increased axial contraction force. Toroidal topologies have been explored for soft robots to generate whole body locomotion [9] and have been used with pressurized fluid to generate anchoring forces [10] [11], but they have not been used for enhanced axial force production.

The presented toroidal soft actuator combines a traditional McKibben actuator with a co-axially located vacuum-style bellow. This design topology enables the expanding fluid volume to be leveraged both in the outward and inward radial directions for axial force production. The resulting actuator is able to produce more force for a given pressure and cross-sectional area. Additionally, the design uses less fluid volume to generate force and displacement than a traditional McKibben actuator, resulting in more efficient overall operation. Section II describes the design in more detail, and Section III models the force of the actuator as a function of the design and operational parameters. Section IV describes the experimental method and resulting data, and Section V includes discussion of the results and potential future work.

II. Design

The toroidal actuator (shown in Figure 1) has a traditional outer McKibben actuator design, constructed with a fluid containing membrane and a fiber reinforcement of helically wrapped fibers at equal and opposite fiber angles. The membrane can be constructed using an elastomer or using an inextensible surface that is at least as large as the fully expanded state of the actuator. Co-axially located within these outer layers is a vacuum-style bellow that creates contraction force through a greater environmental pressure than internal pressure. In the presented design, the inside of the bellow is vented to the outside, maintaining an atmospheric pressure, and the surrounding outer volume is pressurized. This configuration allows a higher pressure differential to be reached in the bellow than with vacuum actuation, as the outer volume can be pressurized well above double atmospheric pressure. To create the inner bellow, an inextensible membrane is placed around rigid spheres; the spheres served to maintain a fixed outer bellow diameter. Using spheres also prevents bellow supports from collapsing, as they cannot be rotated to an unstable configuration.

The resulting design leverages the outward radial expansion of the fluid on the outer fiber reinforcement to generate the same forces that would be created by a McKibben actuator. The inward fluid expansion is captured by the inner bellow and transmitted to the ends, creating additional axial force production; this results in an increase in total force production for a given pressure and cross-sectional area. The toroidal shape also reduces the internal volume that is pressurized during operation of the actuator, improving both the stiffness and efficiency of the actuator.

[1]Josh Bishop-Moser is with Mechanical Engineering, University of Michigan, Ann Arbor, USA josh@bishopmoser.com

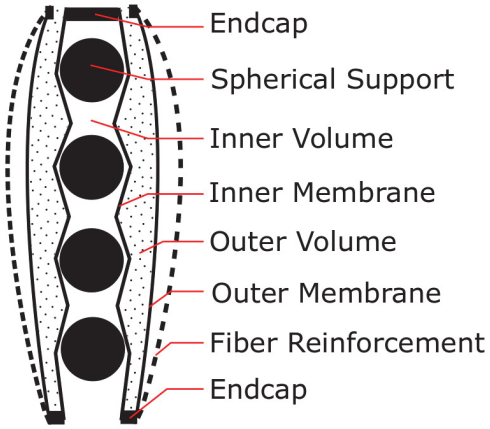

Fig. 1. Cross-sectional diagram of the toroidal actuator showing the inner and outer volumes and membranes, with internal supporting spheres and external fiber reinforcement. The inner volume is at atmospheric pressure, while the outer volume is pressurized. The inner membrane is an inextensible surface, while the outer membrane can be either inextensible or elastic.

The use of spheres as the reinforcing members of the inner actuator presents both advantages and disadvantages in comparison to a traditional vacuum bellow with ring reinforcements. The spheres fully prevent the inner volume from collapsing due to the pressure induced buckling. However, the extra space taken by the spheres along the axial length may reduce the maximum axial displacement of the actuator. Additionally, the increased contact area between the inner membrane and the spheres may reduce force production of the actuator.

A variety of materials can be used to manufacture this design; this paper uses polyethylene sheets that are thermally sealed to form cylinders for the membranes, braided nylon tubing for the fiber reinforcement, and polypropylene hollow spheres for the spherical support.

III. Modeling

The force generation of the toroidal actuator can be modeled using virtual work. Simplifying assumptions about the actuator will be applied to enable the use of this approach, including negligible energy loss into the structure, quasi-static kinematics, and maintenance of a cylindrical shape. Using the virtual work approach, force can be described using Eq. 1, where y is axial displacement, P is pressure, V is volume, and F is force.

$$F = P\frac{\partial V}{\partial y} \tag{1}$$

The instantaneous force of a McKibben actuator using the virtual work method is already known to be Eq. 2 [4], where F_{outer} is the force generated by the outer membrane and the fiber reinforcement, r is the radius of the actuator, and θ is the angle of the reinforcing fibers with respect to the axial direction.

$$F_{outer} = P\pi r^2(1-2\cot^2(\theta)) \tag{2}$$

The volume of the inner bellow is modeled as a pair of truncated cones for each bellow segment. Figure 2 shows the notation used in this derivation.

The length of the inner membrane segment, c_s, is fixed, allowing the indentation of the membrane, x_s, to be found as a function of the segment height, y_s. This is shown in Eq. 3. The equation of a truncated cone is shown in Eq. 4. Substituting Eq. 3 into Eq. 4 provides the inner volume, shown in Eq. 5 as a function of manufactured parameters and the axial length of the segment, y_s. The subscript $_s$ indicates these equations are for a segments of the membrane between the centers of two adjacent spheres; c is the total inner membrane length and y is the total axial length across all segments from endcap to endcap.

$$x_s = \sqrt{c_s^2 - y_s^2} \tag{3}$$

$$V_{inner} = \pi\frac{y_s}{3}(r^2 + (r-x_s)r + (r-x_s)^2) \tag{4}$$

$$V_{inner} = \pi\left(y_s r^2 - y_s r\sqrt{c_s^2 - y_s^2} + \frac{y_s c_s^2}{3} - \frac{y_s^3}{3}\right) \tag{5}$$

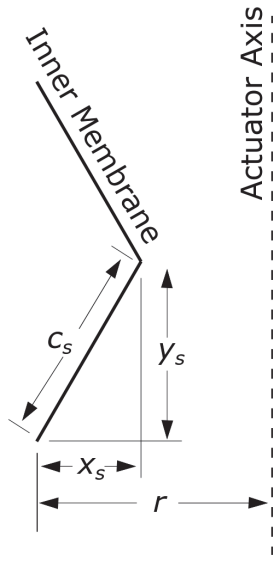

Fig. 2. Notation used in the derivation of the inner volume.

The volume outside of the inner volume (the pressurized volume), can be found as the difference between a virtual cylinder and the inner volume; this volume is shown in Eq. 6.

$$V_{mid} = \pi\left(y_s r\sqrt{c_s^2 - y_s^2} - \frac{y_s c_s^2}{3} + \frac{y_s^3}{3}\right) \tag{6}$$

Plugging Eq. 6 into Eq. 1 and assuming the segments are repeated along the actuator gives the force generation by the inner bellow, shown in Eq. 7.

$$F_{bellow} = P\pi\left(y^2 - \frac{c^2}{3} + \frac{r(c^2-2y^2)}{\sqrt{c_s^2 - y_s^2}}\right) \tag{7}$$

Summing Eq. 2 and Eq. 7 provides the force generation of the toroidal actuator, given the pressure, actuator length, membrane length, fiber angle, and radius; this is shown in Eq. 8.

$$F = P\pi\left(r^2 - 2r^2\cot^2(\theta) + y^2 - \frac{c^2}{3} + \frac{r(c^2-2y^2)}{\sqrt{c^2 - y^2}}\right) \tag{8}$$

This force equation can be used for both analysis and design synthesis of toroidal actuators. As an example of design synthesis, Fig. 3 shows a contour plot of contraction force values for different inner membrane lengths and the fiber angles. The inner membrane alters the shape, and consequently the mechanical advantage, of the inner bellow, while the fibers alter the mechanical advantage of the external reinforcement. The figure shows how equivalent forces can be achieved through different combinations of design parameters. As the fiber angle reaches above approximately 54°, the fiber reinforcement will contribute a net axial extension (a negative axial contraction), and can be offset through the inner membrane length.

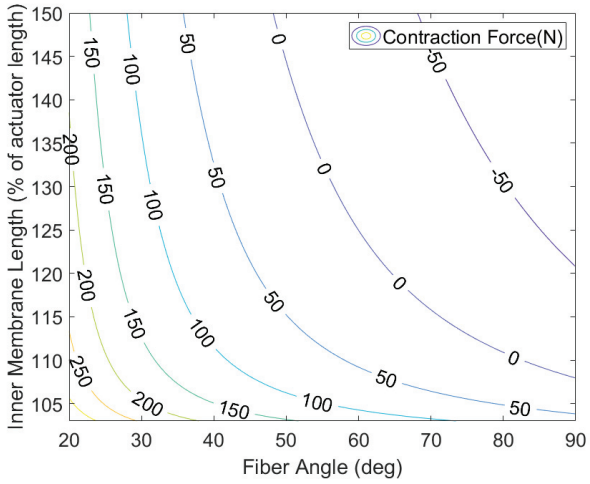

Fig. 3. Contour plot of the contraction force generated by a toroidal actuator as the length of the inner membrane and fiber angle of the external fiber reinforcement vary. Other parameters and variables are fixed as $P = 100$kPa, $r = 0.0127$m, and $y = 0.01$m.

The behavior of a fabricated toroidal actuator can also be analyzed using the force equation. For example, Fig. 4 shows a contour plot of contraction force values over pressure and axial contraction. This shows the operational performance of the actuator, assuming the fiber angle remains constant with contraction.

The spacing of the spheres, driven by the number of spheres, will effect the maximum actuator displacement on one extreme and actuator force on the other. The lower bound of spacing is when $r = y_s$, at which point the spheres

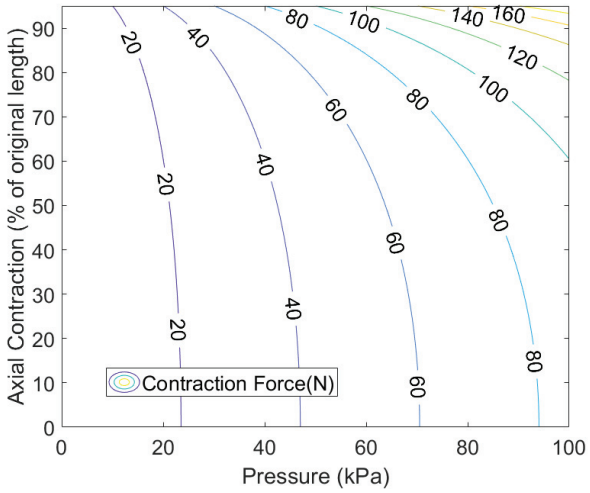

Fig. 4. Contour plot of the contraction force generated by a toroidal actuator over pressure and axial contraction percentage (100% = full manufactured length with no contraction). Other parameters are fixed as $r = 0.0127$m, $\theta = 30°$, and $c = 0.01$m.

are touching end to end, and the actuator cannot contract. The maximum axial contraction as a percentage of actuator length, d_{max}, is shown in Eq. 9. On the other extreme, for large spacing between the spheres, the inner membrane will reach the actuator axis and reduce the overall force generation. This force reduction and the effect of support spacing is detailed more extensively by Felt et al. [7].

$$d_{max} = \frac{y_s - r}{y_s} \tag{9}$$

The radius of the outer membrane and inner membrane were both treated to be equal, as this configuration will maximize force for a given radius. If different radius values are used, Eq. 2 replaces r with r_{out} and Eq. 7 replaces r with r_{in}. The resulting force is shown in Eq. 10.

$$F = P\pi\left(r_{out}^2 - 2r_{out}^2\cot^2(\theta) + y^2 - \frac{c^2}{3} + \frac{r_{in}(c^2-2y^2)}{\sqrt{c^2 - y^2}}\right) \tag{10}$$

IV. Experimental Method and Results

Three actuators were tested for their static force generation:

1) A toroidal actuator
2) A McKibben actuator made from the same materials, dimensions, and manufacturing method as the toroidal actuator
3) A non-fiber toroidal actuator that does not contain the external fiber reinforcement

The toroidal and McKibben actuators enable a direct comparison to determine the change in force generation. The non-fiber actuator provides a measurement of the force generation of the inner bellow in isolation. These actuators are shown in Fig. 5

Fig. 5. a) Toroidal actuator b) McKibben actuator c) Non-fiber toroidal actuator.

A blocking load test is performed over the range of pressures that the materials could handle. Each actuator is placed in an axial measurement device that captures pressure and axial load. The anchoring of the endcaps is fixed in all six degrees of freedom. A Loadstar RAS1-025S Resistive Load Cell is used for force capture. Pressure is swept from 0 to the maximum pressure before material failure; pressure at failure was found experimentally. The pressure is settled at each measurement point for 10 seconds to avoid non-steady state effects. Figure 6 shows the force of the toroidal and McKibben actuators plotted as a function of pressure. Figure 7 shows the force of the non-fiber toroidal actuator plotted as a function of pressure.

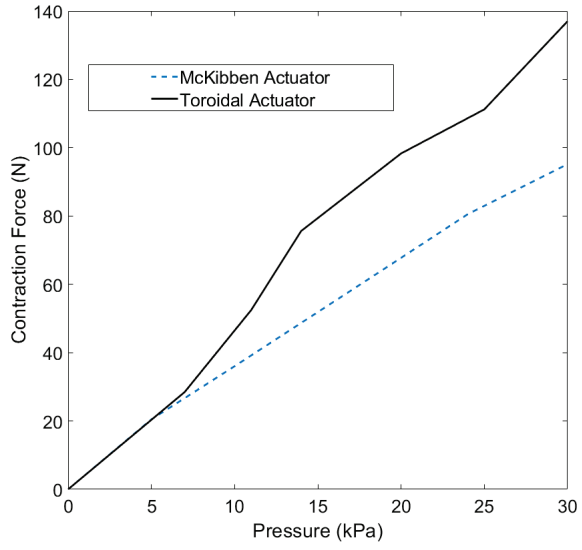

Fig. 6. Measured force value of a toroidal actuator and a McKibben actuator as pressure is swept from 0 to 30 kPa.

The linear regression of the force of the McKibben actuator with respect to fluid pressure has a slope of $3.16\frac{N}{kPa}$, while the force per fluid pressure of the toroidal actuator is $4.58\frac{N}{kPa}$.

The ratio of these values for the toroidal actuator to the McKibben actuator is 1.448, demonstrating that the toroidal actuator generates 44.8% more force than the McKibben actuator for the same pressure and design parameters in a blocking load configuration.

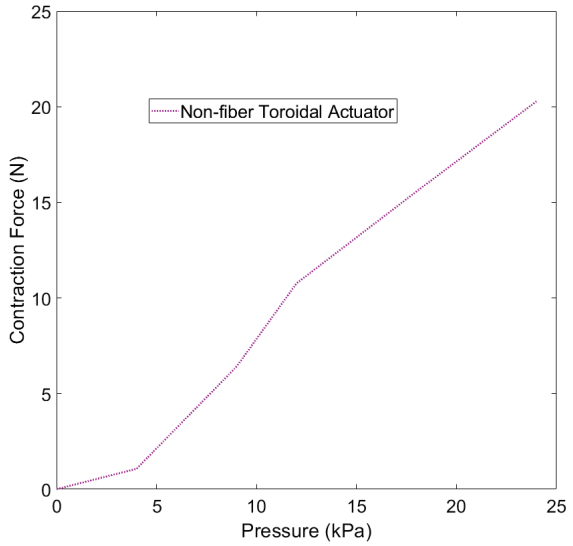

Fig. 7. Measured force value of a non-fiber toroidal actuator as pressure is swept from 0 to 24 kPa.

The model for the toroidal actuator is compared to the experimental values in Fig. 8. The sample prototype dimensions are $r = 0.01778$m, $\theta = 30°$, $y = 0.127$m, and $c = 0.132$m. These values are input into Eq. 8 to find the predicted force values; the negative of the force value is displayed in the plot to show the contraction, rather than the extension force.

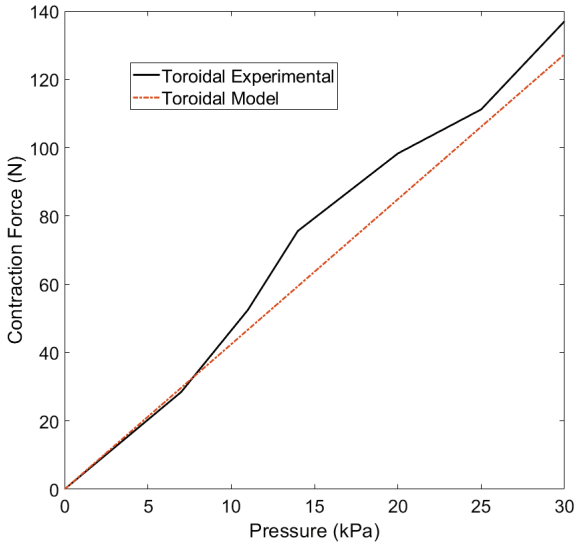

Fig. 8. Measured force value of toroidal actuator compared to the values predicted by the model.

V. Conclusion

This work presents a novel toroidal topology for increased force generation of soft actuators by creating an interior bellow inside a fiber-reinforced actuator. The force is computed analytically using truncated cylindrical pyramid segments to model the inner bellow. The utility of this model for both analysis and synthesis of toroidal actuators is shown through two examples. The toroidal design is experimentally tested for its force production capability over a range of pressures and compared to a traditional McKibben actuator. The toroidal actuator is also tested without the fiber reinforcement to isolate the force generation of the inner bellow component. Key findings for the results include the following:

- The force production is increased over a traditional McKibben actuator by including an interior bellow. For the samples tested, this increase is approximately 45%.
- The model of the force compares favorably with the experimental results, and can be used for analysis and synthesis of toroidal actuators.
- Spheres can be used for the construction of the interior bellow to create a robust and easy to fabricate design.

These findings hold promise for creating high force actuators for soft robotic applications. The presented work looks only at contractile axial motion, but the same concept could be applied to extending, bending, rotating, screw, or other motions in soft actuators. The model had some deviation when compared to the experimental results, which could be due to manufacturing imperfections or oversimplification of the model. It should be noted that more complex modeling of fiber-reinforced actuators [12] and vacuum bellow actuators [7] have been performed and can be applied to refine the model.

Future work in this effort could focus on modeling and experimentally validating the increased stiffness and system efficiency that are expected from this design. Materials that could withstand increased pressure and loads would allow the design to be used to generate higher forces.

Potential applications of this work include soft actuators for human augmentation (e.g., exosuits, rehabilitation robots, orthotics, prosthetics) to apply larger loads to the body without increasing pressure or actuator volume, soft grasping manipulators that can handle larger loads, and mobile robots that can better lift and manipulate both their own body weight and their environment.

References

[1] C.-P. Chou and B. Hannaford, "Measurement and modeling of mckibben pneumatic artificial muscles," *IEEE Transactions on robotics and automation*, vol. 12, no. 1, pp. 90–102, 1996.

[2] J. Bishop-Moser and S. Kota, "Design and modeling of generalized fiber-reinforced pneumatic soft actuators," *IEEE Transactions on Robotics*, vol. 31, no. 3, pp. 536–545, 2015.

[3] W. Felt and C. D. Remy, "A closed-form kinematic model for fiber-reinforced elastomeric enclosures," *Journal of Mechanisms and Robotics*, vol. 10, no. 1, p. 014501, 2018.

[4] J. Bishop-Moser, G. Krishnan, and S. Kota, "Force and hydraulic displacement amplification of fiber reinforced soft actuators," in *ASME 2013 International Design Engineering Technical Conferences and Computers and Information in Engineering Conference*. American Society of Mechanical Engineers, 2013, pp. V06AT07A031–V06AT07A031.

[5] M. A. Robertson, H. Sadeghi, J. M. Florez, and J. Paik, "Soft pneumatic actuator fascicles for high force and reliability," *Soft robotics*, vol. 4, no. 1, pp. 23–32, 2017.

[6] E. W. Hawkes, D. L. Christensen, and A. M. Okamura, "Design and implementation of a 300% strain soft artificial muscle," in *Robotics and Automation (ICRA), 2016 IEEE International Conference on*. IEEE, 2016, pp. 4022–4029.

[7] W. M. Felt, M. A. Robertson, and J. Paik, "Modeling vacuum bellows soft pneumatic actuators with optimal mechanical performance," in *Soft Robotics (RoboSoft 2018), 2018 IEEE-RAS International Conference on*, no. CONF, 2018.

[8] M. D. Lima, N. Li, M. J. De Andrade, S. Fang, J. Oh, G. M. Spinks, M. E. Kozlov, C. S. Haines, D. Suh, J. Foroughi *et al.*, "Electrically, chemically, and photonically powered torsional and tensile actuation of hybrid carbon nanotube yarn muscles," *Science*, vol. 338, no. 6109, pp. 928–932, 2012.

[9] D. W. Hong, M. Ingram, and D. Lahr, "Whole skin locomotion inspired by amoeboid motility mechanisms," *Journal of Mechanisms and Robotics*, vol. 1, no. 1, p. 011015, 2009.

[10] V. Orekhov, M. Yim, and D. Hong, "Mechanics of a fluid filled everting toroidal robot for propulsion and going through a hole," in *ASME 2010 International Design Engineering Technical Conferences and Computers and Information in Engineering Conference*. American Society of Mechanical Engineers, 2010, pp. 1205–1212.

[11] W. Adams, S. Sridar, C. M. Thalman, B. Copenhaver, H. Elsaad, and P. Polygerinos, "Water pipe robot utilizing soft inflatable actuators," in *2018 IEEE International Conference on Soft Robotics (RoboSoft)*. IEEE, 2018, pp. 321–326.

[12] A. Sedal, D. Bruder, J. Bishop-Moser, R. Vasudevan, and S. Kota, "A constitutive model for torsional loads on fluid-driven soft robots," in *ASME 2017 International Design Engineering Technical Conferences and Computers and Information in Engineering Conference*. American Society of Mechanical Engineers, 2017, pp. V05AT08A016–V05AT08A016.